Effect of Nanoparticle Size and Size-Distribution on Mechanical Behavior of Filled Amorphous Thermoplastic Polymers

H. H. Kausch,[1] G. H. Michler[2]

[1]*Institute of Materials, Swiss Federal Institute of Technology Lausanne (EPFL), 1015 Lausanne, Switzerland*
[2]*Institute of Physics, Martin Luther University, Halle-Wittenberg, 06099 Halle/S., Germany*

Received 11 December 2006; accepted 11 January 2007
DOI 10.1002/app.26570
Published online 11 May 2007 in Wiley InterScience (www.interscience.wiley.com).

ABSTRACT: Different types of polymer nanocomposites on the base of polystyrene, polymethylmethacrylate, and polycarbonate with alumina and SiO_2 nanoparticles and carbon nanotubes have been studied. Miniaturized, micro-dimensional samples were used, enabling a good control of morphology and distribution of particles by means of transmission and scanning electron microscopy. Special preparation techniques had been applied, which resulted in a very good dispersion of the nanoparticles. Using these materials with really nanosized particles of a few 10 nm in size the effect on toughness enhancement could be studied without agglomerates as they often appear in the generally used large samples. Micromechanical mechanisms were studied in detail by TEM and SEM investigations of deformed samples. A ''nanoparticle modulated crazing'' could be detected as a toughness enhancing effect. © 2007 Wiley Periodicals, Inc. J Appl Polym Sci 105: 2577–2587, 2007

Key words: nanocomposites; toughness; micromechanical mechanisms; crazes; electron microscopy

INTRODUCTION

Fillers and modifiers have been employed from the very beginning of the industrial use of polymer materials—and about 75 years before the notion of *macromolecule* was born. Fillers are generally used to reduce cost as well as the thermal sensitivity of mechanical properties of the matrix material and to improve—if possible—strength and toughness.

The most important filler parameters influencing the structure and the properties of a polymer matrix are as follows:

particle composition (chemical, mineralogical),
size, size distribution (*top-cut*), and average inter-particle distance,
shape, aspect ratio (spherical, fibrous, plate-like),
particle surface properties (specific surface area, type of bonding that can be engaged with the matrix, affinity to humidity or stabilizing agents, but also nucleation and catalytic activities),
hardness and abrasive action during processing of the compound, dispersion behavior and influence on processing.

When optimizing the above parameters attention must be paid to synergistic effects, but also to indirect and frequently nonlinear effects on polymer structure and mobility.

The addition of particulate, generally stiff fillers influences all stages of the fabrication and service life of the resulting composites:

- processing (viscosity, sedimentation, change of reactivity and heat capacity, dimensional stability);
- structure formation (effects on morphology, density, and optical and electrical properties);
- small strain behavior (elastic moduli, stress concentration, stiffness);
- deformation and rupture (rate of creep, yield stress, composite extensibility and toughness);
- physical and environmental ageing (humidity effects, chemical degradation).

The large spectrum of filler parameters and filler effects makes it sometimes difficult to clearly identify the particular mechanism responsible for an observed effect.

For many applications *toughness* is an important mechanical parameter. For traditional polymer composites containing *micron-sized* fillers it is known that

Dedicated to Prof. Dr. F. J. Balta Calleja on occasion of his 70th birthday.

Correspondence to: G.H. Michler (michler@iw.uni-halle.de).

Contract grant sponsor: Deutsche Forschungsgemeinschaft; contract grant number: DFG: SFB418.

to maintain the generally good toughness of the (semicrystalline) matrix polymer (or to enhance that of the amorphous, brittle matrix polymer) some limiting morphological conditions have to be fulfilled[1]:

1. particle diameter not too large and particle size distribution not too broad,
2. interparticle distance (ID) smaller than a maximum ID^{max} and larger than a minimum distance ID^{min},
3. no strong, perfect interfacial bonding (interfacial strength between particles and matrix), so as to permit partial, localized debonding under load.

If it is assumed that the (spherical) filler particles are homogeneously distributed in the matrix, an average ID or ligament width can be calculated with the mean particle diameter D and filler volume fraction ϕ[2]:

$$\mathrm{ID} = D\left[\sqrt[3]{\frac{\pi}{6\phi}} - 1\right] \quad (1)$$

The above limiting conditions can be represented as a ''toughening window'' in dependence on ID (or D) and interfacial adhesion (Fig. 1).

In all cases of strong adhesion (large interfacial strength) an increase of stiffness and strength can be realized, but as a consequence the toughness K_{Ic} of such composites is low. To achieve good toughness with particulate composites localized debonding and/or particle cavitation seem to be a necessary precondition.[3–5]

Assuming that most of the composite sample strain is born by the (generally much softer) matrix material, a concentration of strain occurs in the ligament areas and the particle-poor regions. The strain level also depends on filler volume fraction. Through the formation of voids by debonding at the particle-matrix interface an enhancement of (fibrillar) deformation of interparticle ligaments is introduced, stored elastic energy consumed and toughness increased. However, the voiding at larger particles and/or the break-up of filler agglomerates generally act as defects, which favor the nucleation and extension of cracks and brittle fracture.

Compared with these traditional polymer composites, a nanoscale reinforcement has attracted more and more attention to improve the properties and stability of polymers. (The term *nanoparticles* refers to inorganic fillers, which exhibit at least one dimension less than 100 nm). These so-called polymer nanocomposites (PNC) exhibit an excellent property profile relevant to a wide diversity of industrial applications, for example, high stiffness, chemical and thermal resistance, dimensional stability, reduced water absorption as well as improved optical or electrical properties, all of which are significantly

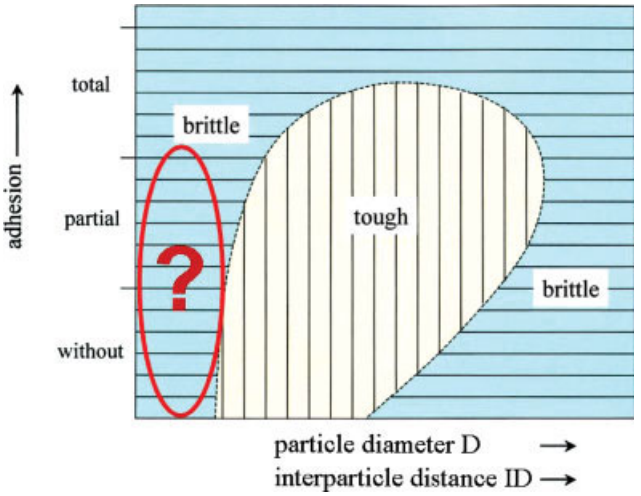

Figure 1 ''Window for toughness'' in a D, ID—interfacial adhesion diagram. [Color figure can be viewed in the online issue, which is available at www.interscience.wiley.com.]

different from those provided by conventional composites.[6]

These in part unexpected properties are certainly related to the two most significant parameters characterizing nanocomposites:

At first, the dimensions of nanoparticles are comparable with the radius of gyration of macromolecules in the polymer matrix. In view of their small size nanoparticles can often be incorporated into the crystalline morphology and/or the network of entangled chains. As a further consequence the average distances ID between nanoparticles are also drastically reduced even at relatively low filler concentrations Φ [eq. (1)], whereas polymer composites with conventional fillers (in the micron range) require loadings of 20 wt % or more to achieve the same effect.

Secondly, the nanoparticles provide ultra-high specific surfaces with (strong) interaction to the polymer matrix. As a consequence of this interaction, structure and/or properties of the matrix polymer are frequently modified, which corresponds to a transition of ''polymer matrix material'' to ''polymer interfacial material.'' With nanofillers the amount of such an interphase relative to the total volume can achieve significant proportions.

Successful high performance PNCs can only be produced, however, if an essential processing requirement is fulfilled, i.e., if particle agglomeration can be avoided through a homogeneous dispersion of nanofillers in the polymer matrix. Particle agglomerates, which are often in the range of micrometers, concentrate the stress and break up readily, which favors

rapid crack propagation, thus leading to brittle fracture and premature catastrophic failure (cf. Fig. 1).

Much more interesting is the question what occurs if particle size D (and interparticle distance, ID) are (much) smaller than 1 μm—this is expressed by the question mark in Figure 1. In the literature, there are several reports showing a decrease of toughness with decreasing particle size (existence of a minimum particle diameter D^{min} or minimum interparticle distance ID^{min} well below the maximum ID^{max}).[7–9] There is a certain probability that in the generally used large samples such agglomerates may have existed, which could in part have accounted for the low toughness values through premature initiation of brittle fracture. In experimental investigations of amorphous PNCs it is particularly important to completely avoid particle agglomerates. Therefore, we wish to study in this work the behavior of amorphous PNCs using miniaturized, micro-dimensional samples with a good control of morphology and dispersion of particles as verified by transmission and scanning electron microscopy.

EXPERIMENTAL

Materials

PS nanocomposites

General purpose polystyrene (GPPS) 158K was supplied by BASF Aktiengesellschaft Ludwigshafen. Alumina nanoparticles used were organically modified boehmite nanoparticles (Disperal OS) supplied by Sasol Germany, Hamburg.

First, GPPS was dissolved in chloroform. The final concentration of the polymer solution was ~ 3%. A calculated amount of filler was weighed out and was added to the polymer solution. A homogeneous, clear suspension was achieved by ultrasonification (VIBRA CELL 75,091 tapered tip, power P = 300 W, duration t = 30 min) of the mixture. Two sets of nanocomposite materials were fabricated containing respectively, 5, 10, 20, and 30% (by weight) of OS.

Subsequently composite films of a thickness of ~ 200 μm were produced by solution casting. The solvent was allowed to evaporate for about two days at room temperature. This procedure was followed by subsequent vacuum drying and annealing under reduced pressure for 24 h at a temperature of 120°C.

Polymethylmethacrylate and polycarbonate nanocomposites

The polymethylmethacrylate (PMMA) nanocomposites modified with 10 and 20 wt % SiO_2 nanoparticles (provided by Röhm and Co. KG) have been prepared by solution blending, as described by Carotenuto et al.[10] The polycarbonate (PC) nanocomposites with 4 wt % multiwalled carbon nanotubes (MWCNTs) were prepared by dilution of a masterbatch of 15 wt % MWCNT in PC (Hyperion Catalysis International Cambridge, MA).[11] The MWCNTs are vapor grown and typically consist of 8–15 graphitic layers wrapped around a hollow 5 nm core. Typical diameters range from 10 to 15 nm, while lengths are between 1 and 10 μm.[12]

Electrospinning of PMMA and PC nanocomposites

To produce polymer nanocomposite fibers via electrospinning (ES), PMMA/SiO_2 and PMMA/MWCNT nanocomposites were dissolved in chloroform at room temperature, with resulting concentrations of 10 and 4 wt %, respectively. To ensure homogeneous solutions for electrospinning, the solutions were vigorously stirred with a magnetic stir bar for at least 10 h at room temperature and were followed by sonification for 30 min. All chemicals were used without further purification. Electrospinning was carried out under ambient temperature in a vertical spinning configuration using a 1-mm inner diameter flat-end needle with a spinning distance of 5 cm. The applied voltages were in the range from 3 to 20 kV, driven by a high voltage power supply (Knürr-Heizinger PNC 30000, Germany). To characterize the fibers, the fibers were directly electrospun onto Cu-grids.[13,14]

Investigations

Morphology

Solution-cast films of PS/alumina nanoparticles were fractured, the resulting fracture surfaces were carbon coated (~ 15 nm) and then investigated by SEM (JEOL JSM 6300). Backscattered electron (BSE) material contrast images were recorded at low magnifications to prove the uniform distribution of the filler over the whole cross-sectional area of the sample. High resolution secondary electron (SE) images were taken at different regions to detect particle size distribution, and to measure interparticle distance.

In addition to studying the morphology of PNCs, ultrathin sections about 50-nm thick were prepared at room temperature using a LEICA ULTRACUT ultramicrotome equipped with a DIATOME diamond knife. The sections were examined by means of transmission electron microscopy (TEM, LEO 912).

For determination of particle size distribution and interparticle distances at least 1000 particles from different regions of each sample were measured manually using an ANALYSIS image processing system. Similarly, interparticle distances were measured considering the next neighbor of each particle.

For characterization the nanofibers, the fibers directly electrospun onto Cu-grids were covered

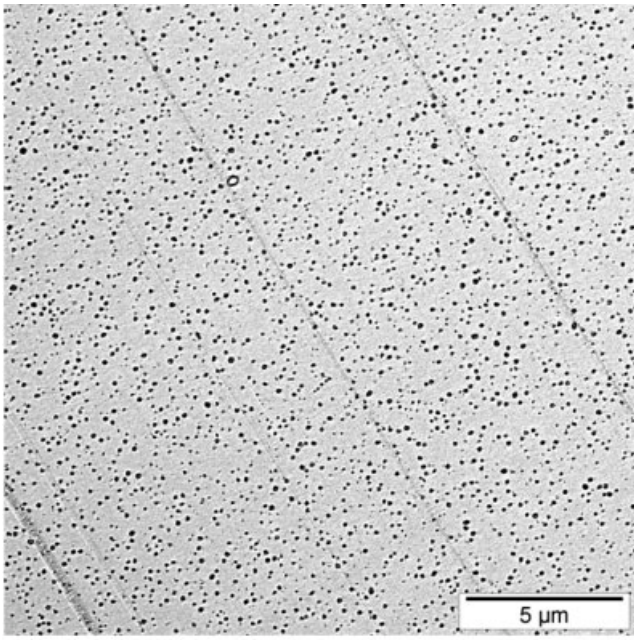

(a)

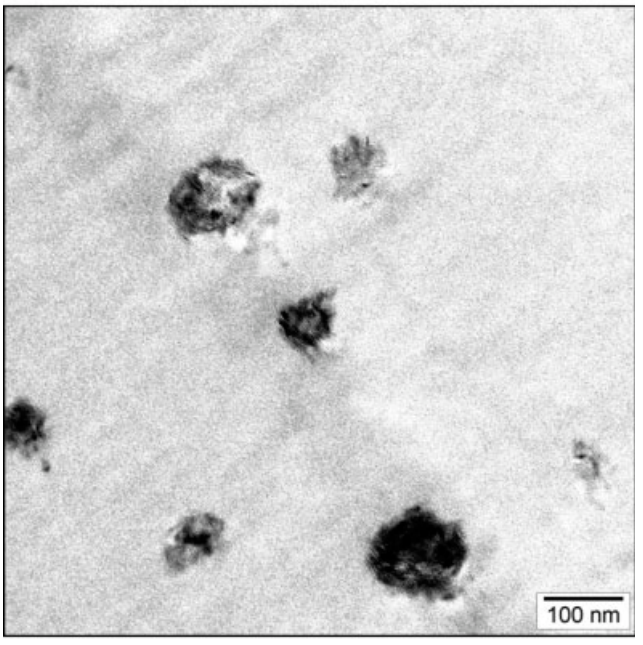

(b)

Figure 2 Morphology of PS/alumina nanocomposite with 5 wt % particles; ultrathin section, TEM (a, b) lower and larger magnification.

with an ultrathin carbon layer, and subsequently investigated by TEM without any chemical staining.

Micromechanical properties

Ultrathin films that are suitable for both TEM and SEM investigations were produced by dip-coating following a procedure proposed by Kramer et al.[15] Foremost, small pieces of the composite films were dissolved in chloroform. A glass slide is dipped into the solution and pulled out slowly in a manner that an ultrathin film is formed. After drying, the film is floated on water surface and transferred to a ductile copper mesh. Subsequently, the copper grids are deformed slowly in tension (MINIMAT materials tester, 0.2 mm/min) until deformation structures—

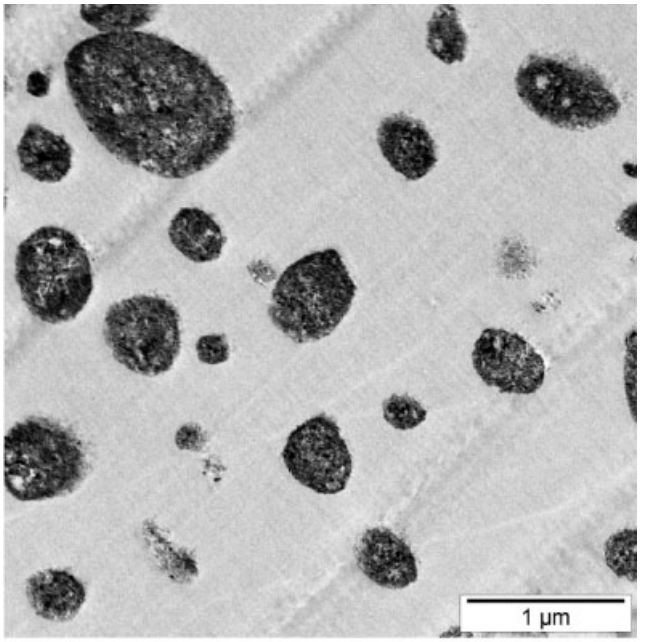

(a)

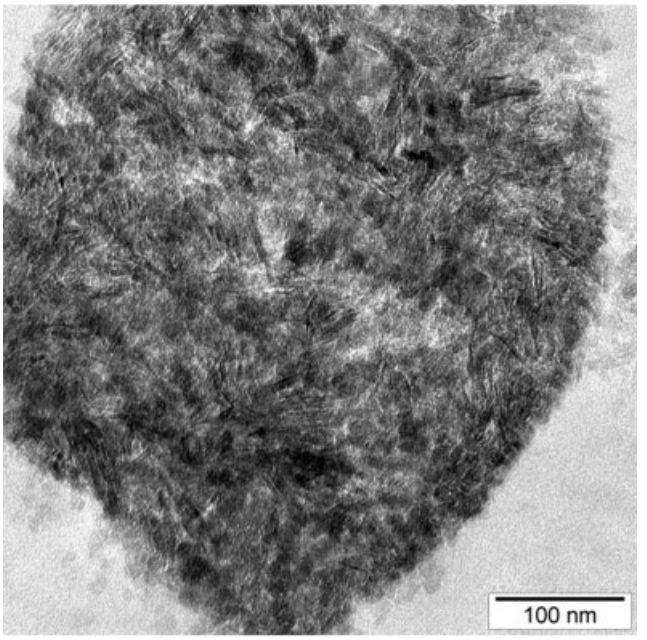

(b)

Figure 3 Morphology of PS/alumina nanocomposite with 30 wt % particles; ultrathin section, TEM (a, b) lower and larger magnification.

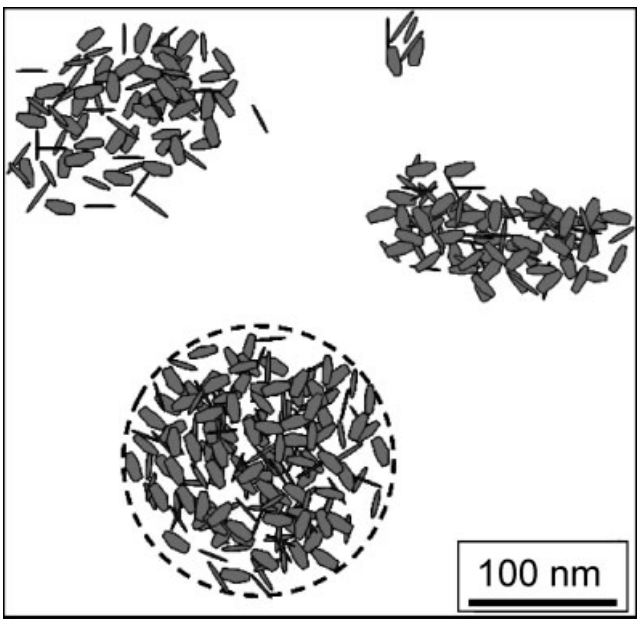

Figure 4 Schematic illustration of the formation of spherical agglomerates by aggregation of primary alumina nanoparticles.

such as crazes and/or cracks, become visible. Because of the plastic deformation of the supporting copper grid, the deformation state of the film is fixed. Finally, the deformed ultrathin films were investigated by means of scanning and transmission electron microscopy.

RESULTS AND DISCUSSION

PS/Alumina nanocomposites

The primary alumina nanoparticles have a minimum size of less than 100 nm. In the composite with a total amount of 5 wt % most particles visible in Figure 2 show this minimum size with only a small number of agglomerated structures having a size of up to about 200 nm.

With increasing particle content more and more particle agglomerates appear with a shift of the maximum particle size to larger values. The nanocomposite with 30 wt % particles shows spherical agglomerates of up to above 1 μm with an average size of about 0.7 μm (Fig. 3).

This agglomeration of the primary particles is schematically illustrated in Figure 4. Increase in the size of agglomerates as well as shift of average size to larger values is shown in the frequency distributions of Figure 5.

It is a noteworthy result that larger agglomerates with a size above 400 nm appear only at higher filler content of 30 wt % and more.

Deformation tests of these PS/Alumina nanocomposites reveal an interesting modification of craze initiation behavior in PS. Lower magnifications of a deformed thin film in the SEM show the usual craze pattern with fibrillated crazes (Fig. 6). The craze structure is modulated by larger nanoparticle agglomerates, which generate larger voids by debonding and partly coarser fibrils between them. The larger magnification of Figure 7 demonstrates the interrelation between alumina particles, debonding, nanovoid formation, and fibrillation. With increasing particle content larger agglomerates appear, creating larger voids inside the crazes (Fig. 8).

The modulated craze structures visible in Figures 6–8 reveal a modified crazing mechanism as compared with the usual mechanism in PS: as sketched in Figure 9, particle agglomerates are breaking up and/or are debonded from the PS matrix, generating

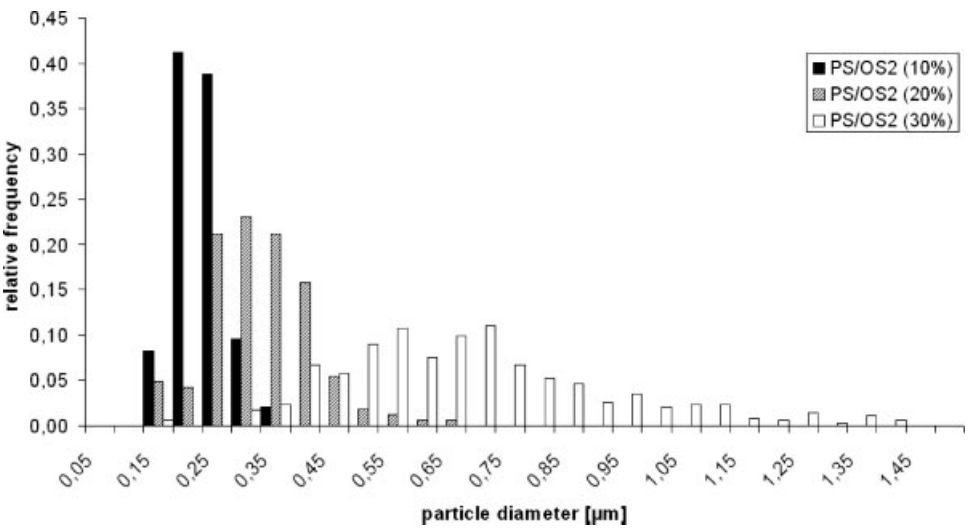

Figure 5 Frequency distribution of the size of observed nanoparticle structures (primary particles and agglomerates) in PS/alumina nanocomposites with increasing filler content.

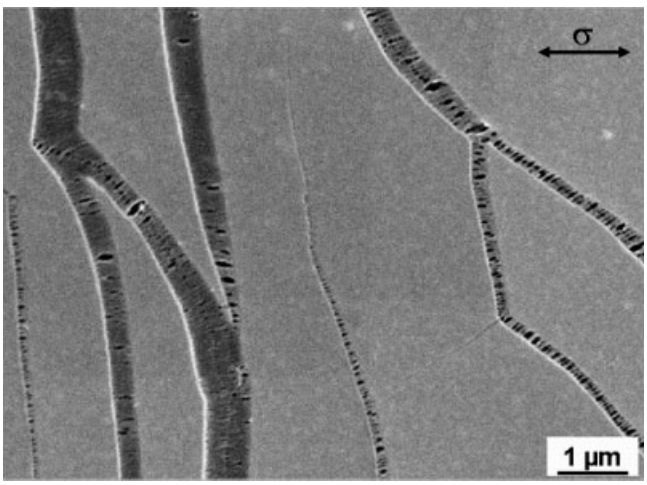

Figure 6 Crazes in PS/alumina nanocomposite with 5 wt % particle content. Craze structure is modulated by nanoparticle agglomerates, generating larger voids inside the fibrillated crazes. Solution-cast film, deformed, SEM.

smaller or larger voids; the PS strands in the voided structure are then stretched into fibrils. Here, the breaking up or debonding stress determines the crazing stress, which is lower than that in unmodified PS. Therefore, slight agglomeration makes crazing easier and more crazes can be created with a positive effect on toughness. A more detailed discussion of the influence of nanofiller concentration on the size of possible particle agglomerations and on the resulting deformation mechanisms of PS/boehmite nanocomposites will be given elsewhere.[16]

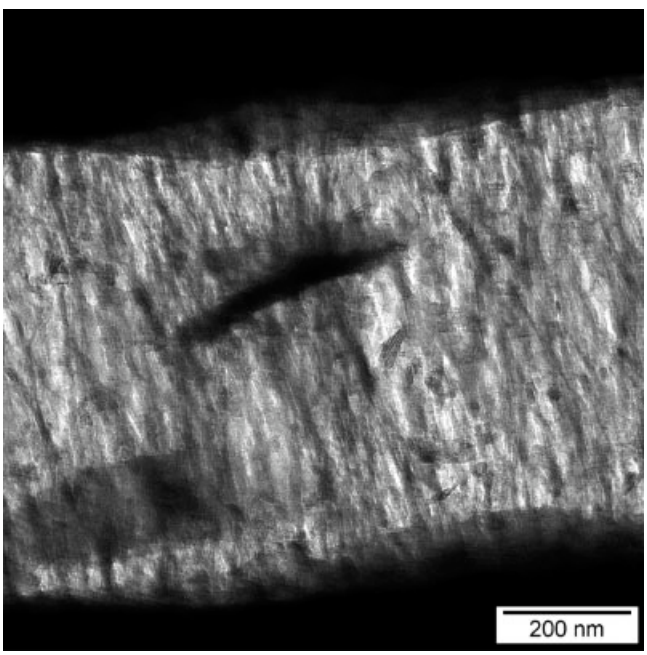

Figure 7 Internal structure of a craze in PS/alumina nanocomposite with 10 wt % particle content: debonded particles, nanovoids, and fibrils. Solution-cast film, deformed, TEM.

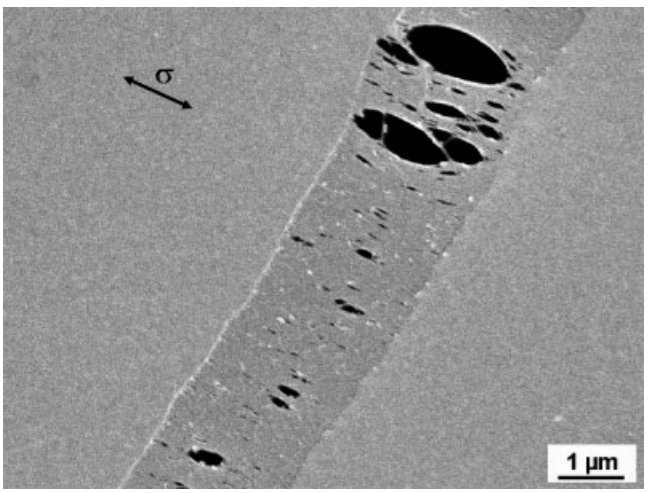

Figure 8 Craze in PS/alumina nanocomposite with 20 wt % filler: Particle agglomerates generate larger voids. Solution-cast film, deformed, SEM.

PMMA/SiO_2 nanocomposites

Figure 10(a) shows the phase morphology of a PMMA/SiO_2 nanocomposite in a 50 nm ultrathin section with 10 wt % SiO_2. The SiO_2 nanoparticles appear uniformly dispersed in the PMMA matrix without any evidence of agglomeration. The average diameter is 26 nm, and the particle sizes exhibit a well-defined Gaussian distribution[17] [Fig. 10(b)]. As a consequence of the small particle size, this nanocomposite reveals excellent optical properties. Light

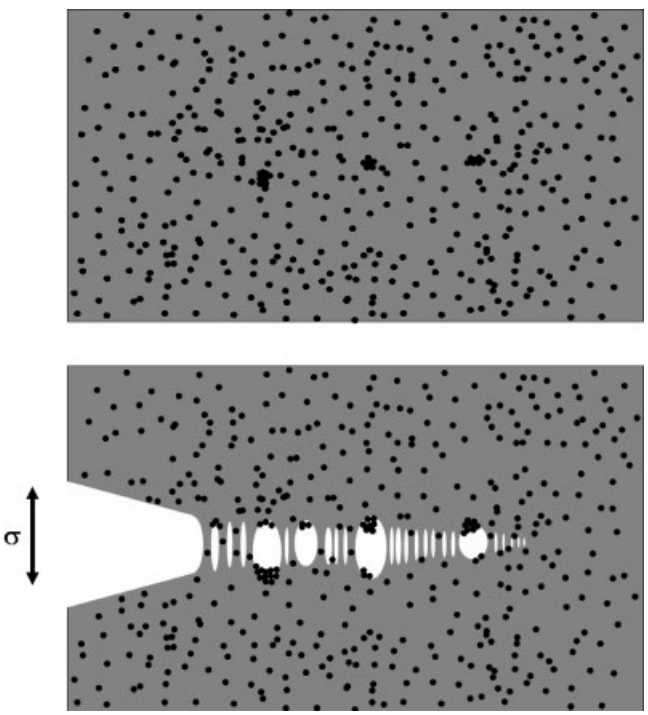

Figure 9 Schematic representation of craze formation in a PS/alumina nanocomposite.

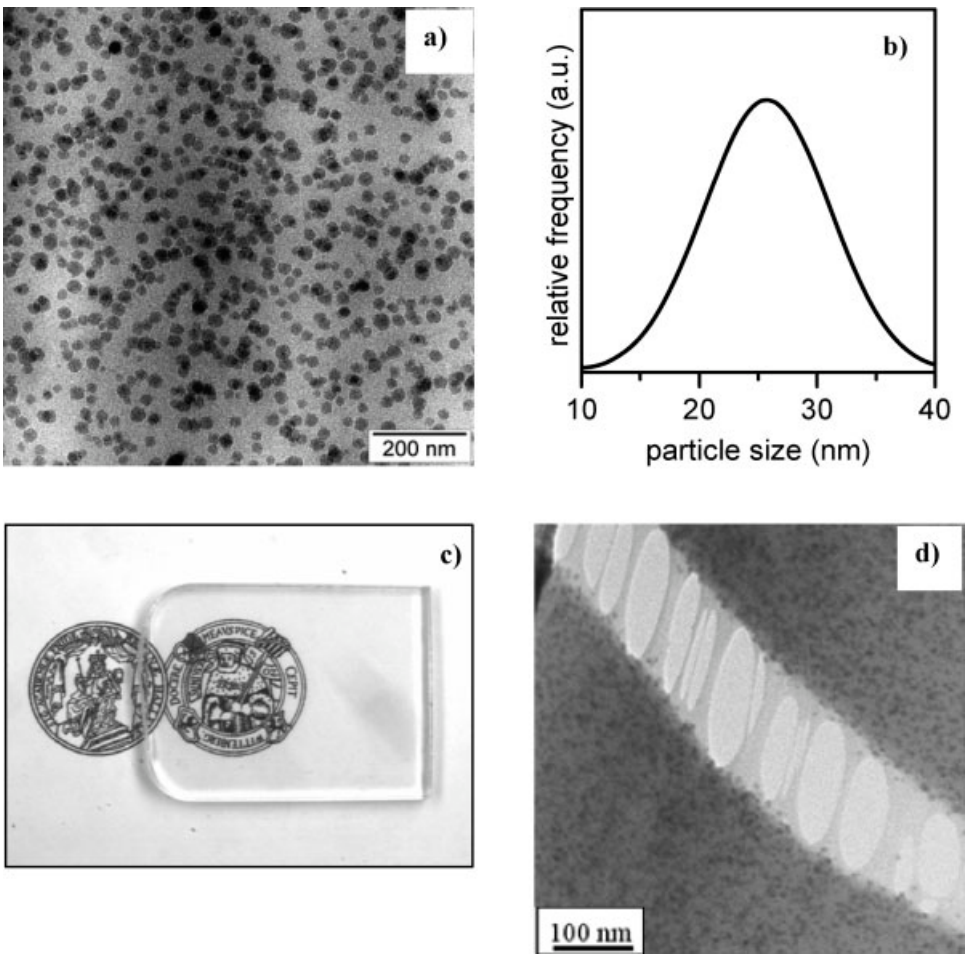

Figure 10 (a) Phase morphology of PMMA nanocomposite with 10 wt % SiO_2; (b) SiO_2 particle size distribution; (c) optical characteristics of PMMA nanocomposite with 20 wt % SiO_2; (d) deformation structure of PMMA nanocomposite with 10 wt % SiO_2 under uniaxial tensile load, [(a, d) ultrathin sections, TEM].

transmission is not affected by the presence of SiO_2 nanoparticles, even at up to 20 wt % of filler content [Fig. 10(c)]. The *in situ* TEM investigation of the micro-deformation behavior of thin films of PMMA with 10 wt % SiO_2 [Fig. 10(d)] shows that classical crazes with nanovoids and fibrillar strands of deformed PMMA matrix material are formed; the latter are still containing some nanoparticles.

The same material (PMMA with 10 wt % SiO_2) had also been transformed into nanocomposite fibers by electro-spinning [Fig. 11(a)]. One clearly sees that the SiO_2 nanoparticles are relatively uniformly dispersed within the (undrawn) fiber. The observed fibers have on the average a diameter of about 100 nm. The diameter as well as the particle distribution show a certain variation along the fiber axis. It should also be noted that the PMMA matrix material is uniaxially oriented during the spinning process. When exposed to traction, strain concentration occurs in the particle-poor regions eventually leading to a ductile deformation zone [Fig. 11(b)]. The fact that the electrospun nanofibers deform under tensile load in a ductile manner, as clearly recognized in this TEM picture, is in contrast to the (craze-like deformation and brittle) behavior of bulk PMMA/SiO_2 nanocomposites. It must be concluded, therefore, that the intrinsic brittleness of the isotropic bulk nanocomposite is completely suppressed by the state of partial molecular orientation of the matrix material and by the lack of lateral confinement in a nanofiber. This observation is another evidence of thin layer ductility as mentioned earlier and discussed in the literature.[18,19]

PC/MWCNT nanocomposites

The phase morphology of PC/multiwalled carbon nanotube (MWCNT) composites as taken by TEM is shown in Figure 12(a). Here one can recognize that the MWCNTs are dispersed in form of a highly entangled (interconnected network) structure in the PC matrix. The MWCNTs used in this study exhibit distinctly curved shapes, which can be described as ''spaghetti'' like structure ultimately forming an

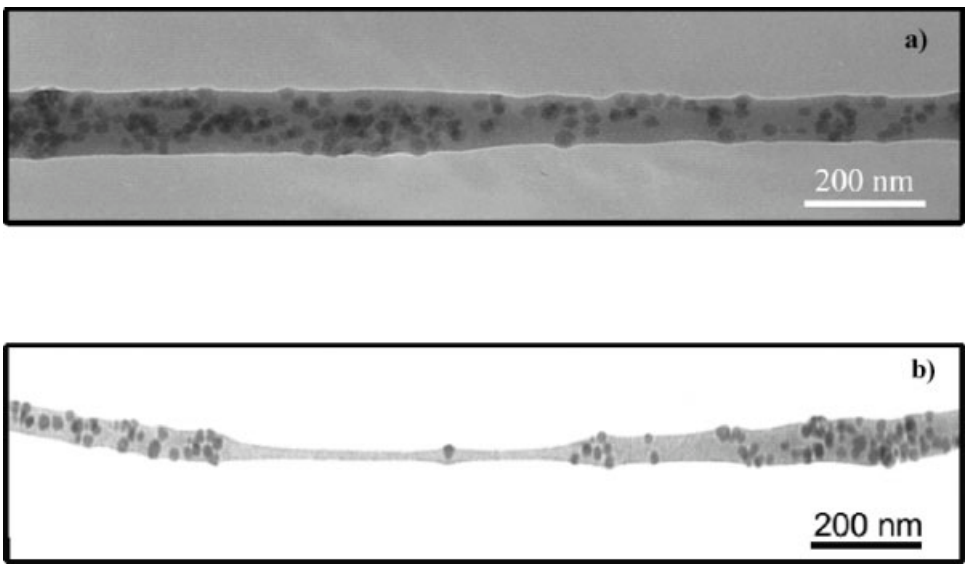

Figure 11 *In situ* TEM micrographs of the mechanical deformation process of an electro-spun PMMA/SiO_2 nanocomposite; (a) before deformation, and (b) fiber deformed under uniaxial tensile load to beyond a critical strain.

interlocked microstructure of MWCNT in the agglomerated state. An *in situ* uniaxial tensile test in TEM of a solution cast film at room temperature [Fig. 12(b)] reveals that the PC/MWCNT nanocomposite film deforms by fibrillated crazing. This behavior is clearly different from that of pure PC, which deforms through shear yielding,[20] and must be ascribed to the presence of the stiff nanotubes of high aspect ratio.

The explanation resides in the axial- and bending-stiffnesses of the MWCNTs, which gives rise to a strong resistance of the interconnected network of nanotubes to lateral contraction and to the stress concentration at the fiber ends which favors void formation.

To analyze the behavior of such nanocomposites use can be made of the model developed by Hsiao almost 50 years ago for a network of linear, elastic, stiff elements.[21]* In a subsequent paper Kausch-Blecken von Schmeling and Hsiao[22] had derived the Young's modulus E' of an isotropic network as a function of the elastic properties of the constituent linear elements:

$$E^{|} = \kappa\rho L^2/6 \tag{2}$$

where L and κ are the length and elastic constant of the orienting elements respectively, and ρ a function describing their volume concentration and orientation distribution. If such a stiff and contiguous network is embedded in a matrix, the macroscopic Young's modulus E_c of the composite is written as:

$$E_c = T_t\kappa\rho L^2/6 + E_m \tag{3}$$

with T_t being a constant quantifying stress transmission from the matrix to the linear elements and E_m the matrix modulus.

From the model a Poisson's ratio close to 0.25 is derived and as a consequence elastic uniaxial strain gives rise to pronounced volume dilation and hydrostatic tension, which favor cavitation followed by fibrillar deformation of the ligaments—as it is seen in Figure 12(b). The formation of voids during the transformation of the isotropic nanocomposite into highly uniaxially oriented tapes by hot drawing is an obstacle, which can be overcome, however, by hot compaction. Prominent research of the science and technology of this technique and careful analysis of the orientation behavior has been done by Ward et al.[23,24] In a recent review[25] the properties of carbon nanotubes, the requirements of composite processing and the theory of fiber-reinforced composite materials are more extensively discussed.

It should be emphasized that despite the extensive formation of nanopores during electro-spinning our *in situ* TEM experiments did not reveal any sign of lateral debonding of the embedded nanotubes from the matrix. The individual MWCNTs become well aligned within the highly deformed fibers. This suggests that the stress transfer at the interface between

*Before the discovery of chain folding in 1957 it was believed that the orientation behavior of macromolecular solids was determined by the rotation of strongly anisotropic micellar domains whose elastic properties were dominated by the stiffness of extended chain segments. From their aggregate models Ward and Kausch deduced later that the rotating domains were very much larger (and much less anisotropic) than a few extended chain segments oriented in parallel.

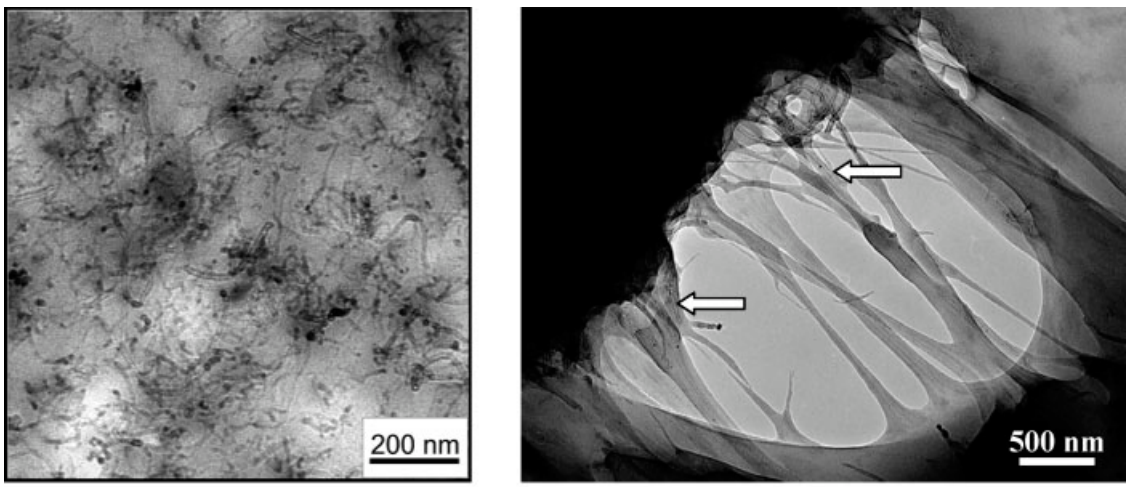

Figure 12 Typical phase morphology (a) and deformation structure (b) of a PC/MWCNT nanocomposite (arrows indicate the areas where the MWCNTs are embedded in fibrils).

nanotubes and matrix is sufficiently high and does not suffer from the extensive local deformation. The craze fibrils of the PC/MWCNT nanocomposites are reinforced by the embedded MWCNTs, which contributes further to an effective stress transfer across the craze zone and to plastic deformation—and toughness—of the PNCs.

Role of particle size and interparticle distance

It is well established that the interparticle distance between dispersed particles plays a crucial role in the toughening mechanism in heterogeneous polymer systems (e.g.,[2,4,8,17,20,23,26]). This interparticle distance (ID) as function of particle size (D) and its volume fraction can be readily estimated by eq. (1) and is illustrated by Figure 13.

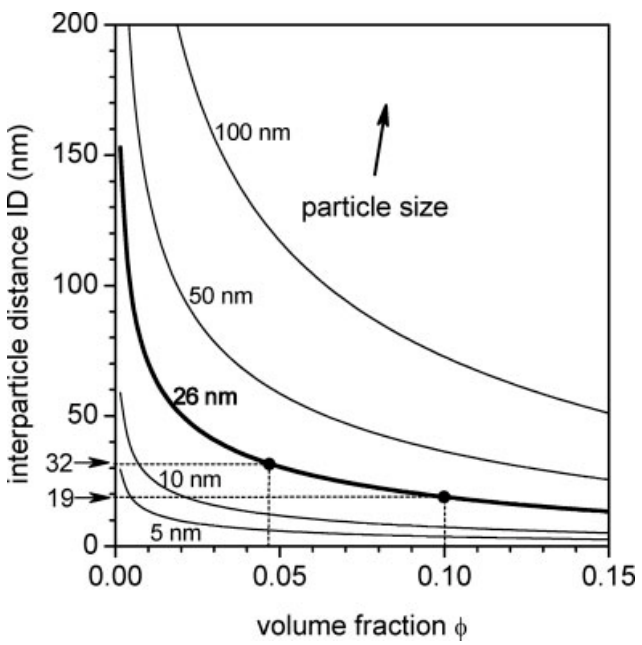

Figure 13 Interparticle distance ID as a function of particle size and volume fraction of particles.

At a given particle size D, it is clear that the interparticle distance decreases as the filler volume fraction increases. The data used in our investigated nanocomposites are compiled in Table. I.

It is also seen from Figure 13 and Table I that, by reducing the particle size from micrometer to nanometer the possibly present interfacial layer around the particles becomes more important because of the enormously high specific surface area. The characterization of such interfacial layers is not trivial and it depends extensively on measuring techniques. For instance, in the present work, we have analyzed the thickness d_l of the interfacial layer in the PMMA/SiO_2 nanocomposites using DSC measurements,

TABLE I
Comparison of Average Particle (Agglomerate) Diameter (D) and Average Interparticle Distance (ID) of Investigated Nanocomposites

Sample	Vol. content	Average particle diameter D	Average distance ID
PS/5 wt.-% Alumina	2.3 vol.-%	150 nm	210 nm
PS/10 wt.-% Alumina	4.8 vol.-%	200 nm	200 nm
PS/20 wt.-% Alumina	10.2 vol.-%	300 nm	190 nm
PS/30 wt.-% Alumina	16.3 vol.-%	660 nm	210 nm
PMMA/SiO_2 10 wt.-%	5 vol.-%	26 nm	32 nm
PMMA/SiO_2 20 wt.-%	10 vol.-%	26 nm	19 nm
PC/MWCNT 4 wt.-%	2 vol.-%	10–15 nm	–

which gave an estimate for d_l of approximately 9 ± 3 nm.[17] Therefore, in PMMA with 5 vol % SiO_2 nanoparticles (which corresponds to 10 wt %), the calculated interparticle distance ID is 32 nm and, if we subtract the effective particle boundary layers ($d_l \sim 9$ nm), then the remaining ligament ID-2d_l has a thickness of about 14 nm. Such ligaments 14 nm thick can apparently be highly stretched in form of craze fibrils [Fig. 10(d)]

At a 10% volume fraction of SiO_2 nanoparticles (same as 20 wt %), the interparticle distance ID is 19 nm and with the same size of the boundary layer of $d_l \sim 9$ nm, the ligament thickness ID - $2d_l$ becomes nearly zero. This means that the boundary layers of neighboring particles touch each other and a percolation of the interfacial layers takes place at this volume fraction indicating that the deformation process of the nanocomposite is entirely controlled by the properties of the more mobile interfacial material. Accordingly the reduction of the interparticle distance to below 14 nm should result in a decrease of composite toughness. In fact the fracture toughness values of PMMA, PMMA/5 vol % SiO_2 and PMMA/10 vol % SiO_2 have been determined as 30, 67, and 48 MPa $\sqrt{\text{mm}}$, respectively.[17]

In all of our nanocomposites PS/alumina, PMMA/SiO_2, PC/MWCNT (exclusive the electrospun nanofibers) the deformation mechanism is the modulated crazing: nanoparticles favor the initiation of nanovoids leading to stress concentration in the adjacent matrix strands, to yielding and fibrillation of the matrix polymer. The size of the voids inside the cavitated/fibrillated craze structure depends on the size of nanoparticles or agglomerates of particles.

The easy debonding of particles from the matrix polymer generates easy cavitation, reducing the effective stress for crazing. Therefore, this type of ''nanoparticle modulated craze'' acts as a source of additional toughness enhancement. This qualitative result could be quantitatively confirmed with the PMMA/SiO_2 nanocomposites.[17] Some questions remain for additional investigations, such as to know the optimum particle diameter and the optimum interparticle distance (or optimum weight/volume content of particles).

In Table I calculated average distances ID between particles or agglomerates are compared. For the PS/alumina nanocomposites the average distances change little (about 200 nm), since with increasing particle content the average agglomerate size increases, too. However, the typical fibril thickness of the modulated crazes are smaller (Fig. 7). That means that also smaller particles initiate nanovoids and fibrillation.

In the PMMA/SiO_2 nanofibres a homogeneous yielding of the PMMA matrix strands between the SiO_2 particles was found instead of crazing as in bulk samples. This shows that we have here a transition from crazing with cavitation/fibrillation to homogeneous yielding with a thin layer yielding mechanism, discussed recently.[20] The critical interparticle distance ID for this homogeneous yielding is about 32 nm (including the both boundary layers of 2 × 9 nm, see Table I and Fig. 13) and, therefore, somewhat larger than observed for PS in SBS-blockcopolymers.[18]

CONCLUSIONS

1. To study the effect on mechanical properties a good dispersion and separation of nanosized particles without formation of larger agglomerates is necessary; this was achieved using solution blending or electro-spinning techniques.
2. Limited interfacial adhesion enables debonding and nanovoid formation during mechanical loading. Because of the local stress concentration at the nanovoids, adjacent polymer matrix strands can be brought to plastic yielding. The combined process of nanovoid enlargement and extension of matrix strands into fibrillar matter are very similar to the mechanism of crazing in amorphous polymers (PS, PMMA, PC).
3. In thin electro-spun nanofibers nanoparticles are dispersed in a matrix without lateral constraint, which facilitates homogeneous yielding of (the PC) matrix material (corresponding to the thin-layer yielding mechanism observed in PMMA).
4. Interparticle distances in the range of a few 10 nm give rise to the mechanism of nanoparticle-modulated crazing in nanofilled PS, PMMA and PC. In PMMA/SiO_2 nanocomposites the fracture toughness K_{Ic} increases from 30 MPa $\sqrt{\text{mm}}$ of neat PMMA up to 67 MPa $\sqrt{\text{mm}}$ for a composite with 5 vol % SiO_2 nanoparticles, corresponding to an interparticle distance of 32 nm. Interparticle distances in nanoparticle filled nanofibers also lie around 32 nm, i.e., the resulting matrix strands are able to deform homogeneously without lateral constraints exerted within the fibers.
5. Both mechanisms of nanoparticle-modulated fibrillar crazes as well as of homogeneous thin-layer yielding increase toughness of the material without significant reduction of stiffness and strength. Therefore, nanocomposites based on amorphous polymer matrices with well-separated nanoparticles reveal true toughening mechanisms. As opposed to that, nanocomposites having larger agglomerates tend to initiate voids acting as crack nuclei and, as a consequence, show brittle behavior through rapid crack propagation.

The authors thank Röhm, Darmstadt, Sasol Germany, Hamburg, and P. Pötschke in the IPF Dresden for kindly having supplied materials and samples; the authors par-

ticularly thank S. Henning and G.-M. Kim for experimental work done at the University.

References

1. Michler, G. H. Kunststoff-Mikromechanik: Morphologie, Deformations und Bruchmechanismen; Hanser: Munich, 1992.
2. Wu, S. Polymer 1985, 26, 1855.
3. Kinloch, A. J.; Guild, F. J. In Toughened Plastics II; Riew, C. K., Kinloch, A. J., Eds.; American Chemical Society: Washington, DC, 1996; pp 1–25, .
4. Kim, G.-M.; Michler, G. H. Polymer 1998, 39, 5689.
5. Schirrer, R.; Fond, C.; Lobbrecht, A. J Mater Sci 1996, 31, 6409.
6. Pinniavaia, T. J.; Beall, G, Eds. Polymer Clay Nanocomposites; New York: Wiley, 2001.
7. Bartczak, Z.; Argon, A. S.; Cohen, R.E.; Weinberg, M. Polymer 1999, 40, 2331.
8. Bartczak, Z.; Argon, A. S.; Cohen, R. E.; Weinberg, M. Polymer 1999, 40, 2347.
9. Sanden, V. d. M. C. M.; Buijs, L. G. C.; Bie, F. O.; Meijer, H. E. H. Polymer 1994, 35, 2783.
10. Carotenuto, G.; Nicolais, L.; Kuang, X.; Zhu, Z. Appl Comp Mater 1995, 2, 385.
11. Ferguson, D. W., Bryant, E. W. S.; Fowler, H. C. ANTEC'98 1998, 1219.
12. Kim, G.-M.; Michler, G. H.; Pötschke, P. Polymer 2005, 46, 7346.
13. Kim, G.-M.; Lach, R.; Michler, G. H.; Pötschke, P.; Albrecht, K. Nanotechnology 2006, 17, 963.
14. Kim, G.-M.; Lach, R.; Michler, G. H.; Chang, Y.-W. Macromol Rapid Commun 2005, 26, 728.
15. Kramer, E. J.; Berger L. L. In Fundamental Processes of Craze Growth and Fracture; Kausch, H.H., Ed.; Springer-Verlag: New York; 1990; Adv Polym Sci 1990, 51/52, 1.
16. Henning, S.; Adhikari, R.; Michler, G. H., in preparation.
17. Lach, R.; Kim, G.-M.; Michler, G. H.; Grellmann, W.; Albrecht, K. Macromol Mater Eng 2006, 291, 263.
18. Michler, G. H.; Adhikari, R.; Lebek, W.; Goerlitz, S.; Weidisch, R.; Knoll, K. J Appl Polym Sci 2002, 85, 683.
19. Michler, G. H.; Kausch, H. H.; Adhikari, R. J Macromol Sci Part B: Phys 2006, 25, 1.
20. Kim, G.-M.; Lach, R.; Michler, G. H.; Pötschke, P.; Albrecht, K. Nanotechnology 2006, 17, 963.
21. Hsiao, C. C. J Appl Phys 1959, 30, 1492.
22. Kausch-Blecken von Schmeling, H. H.; Hsiao, C. C. J Appl Phys 1968, 39, 4915.
23. Ward, I. M.; Hine, P. J. Polymer 2004, 45, 1413.
24. Hine, P. J.; Broome, V.; Ward, I. M. Polymer 2005, 46, 10936.
25. Coleman, J. N.; Khan, U.; Blau, W. J.; Gun'ko, Y. K. Carbon 2006, 44, 1624.
26. Chabert, E.; Chazeau, L.; Gauthier, C.; Dendievel, R.; Cavaillé, J. Y. Mécanique et Industries 2004, 5, 489.